Available online at www.sciencedirect.com
ScienceDirect
Trans. Nonferrous Met. Soc. China 31(2021) 1828−1841
Transactions of Nonferrous Metals Society of China
www.tnmsc.cn

One-step and selective extraction of nickel from nickel-based superalloy by molten zinc

Qing-hua TIAN[1,2,3], Xiang-dong GAN[1,2,3], Da-wei YU[1,2,3], Fu-hui CUI[1,2,3], Xue-yi GUO[1,2,3]

1. School of Metallurgy and Environment, Central South University, Changsha 410083, China;
2. National & Regional Joint Engineering Research Center of Nonferrous Metal Resources Recycling, Changsha 410083, China;
3. Hunan Key Laboratory of Nonferrous Metal Resources Recycling, Changsha 410083, China

Received 3 June 2020; accepted 28 December 2020

Abstract: Nickel-based superalloy was treated with molten zinc for the selective extraction of nickel. The effects of heating temperature, heating time, and the mass ratio of zinc to superalloy on the extraction of metals in the superalloy were investigated. An extraction rate of 95.2% for nickel, 55.4% for iron and 30.4% for chromium, but low extraction rates of the refractory metals (titanium (Ti), molybdenum (Mo), and niobium (Nb)) were obtained under the optimal conditions of the heating temperature of 850 °C, the heating time of 4 h, and the zinc/superalloy mass ratio of 10:1. In the subsequent vacuum distillation process, the obtained nickel alloy contained nickel with a purity of 73.5 wt.% after zinc removal. Moreover, the recovered zinc after the distillation process had a purity of 99.9 wt.%. The results of the investigated process indicated the possibility of extracting nickel directly from nickel-based superalloy scraps.
Key words: superalloy; zinc; nickel; extraction; vacuum separation

1 Introduction

Superalloys are advanced high-temperature materials with iron, nickel, or cobalt as the matrix metal with excellent high-temperature strength, fatigue resistance, fracture toughness, and other comprehensive properties. They have been widely used in aerospace, nuclear power generation, petrochemical industry, ship manufacturing, and other fields [1,2]. The market for superalloys has recently reached an unprecedented growth trajectory due to the enormous demand in China's industrial revolution. According to data from the National Bureau of Statistics (NBS), the international market consumed about 300000 t of superalloy materials in 2018, and the annual demand for superalloy in China was over 20000 t, with an average annual growth rate of 15%. Because of the finite service life of superalloys and the scraps generated in the machining process, the superalloy scraps gradually increase [3,4].

As a vital secondary resource for extracting valuable metals, the superalloy scraps, can be treated with various processes, which can be divided into three categories: pyrometallurgy, hydrometallurgy, and pyro-hydrometallurgy. Scraps containing a few impurities and distinctive alloy composition are re-melted with original alloying metals to produce initial superalloy ingots [5,6]. The discarded parts are typically pre-treated to remove heat-resistant coating (ZrO_2 or Al_2O_3) by acid dissolution and/or mechanical polishing. However, the quality control of the superalloy is

Corresponding author: Da-wei YU, Tel: +86-731-88876255, E-mail: dawei.yu@csu.edu.cn;
Fu-hui CUI, Tel:+86-18642067797, E-mail: fuhuicui@csu.edu.cn
DOI: 10.1016/S1003-6326(21)65620-0

difficult due to the uncertain composition of the added superalloy scraps, even if the composition of the superalloy is subject to strict quality control. Therefore, the quantity of the added superalloy scraps for re-melting is limited [7,8]. Scraps with high amounts of impurities are mainly used as additives in the production of steel and other metals, leading to the loss of rare and expensive metals such as Re and Ta [9]. Hydrometallurgy usually adopts the acid dissolution, such as HCl (with Cl_2 gas) [10−12], H_2SO_4 [13,14] or HCl+HNO_3 [15,16], to dissolve superalloy scraps into aqueous solutions, followed by the separation and purification using extraction, precipitation and ion exchange, to achieve the purpose of recycling and reuse. The cobalt recovery can reach above 90% and that of nickel above 95% using hydrometallurgical processes. Pyro-hydrometallurgy often uses pre-treatment, such as alkali melts [17], oxidation [18] or low-melting metals (such as Al [19], Zn [20]) to modify the characteristics of the superalloy (i.e., high hardness and excellent stability), followed by a series of hydrometallurgical methods to realize the extraction and recovery of alloy elements.

The existing recycling processes of superalloy scraps have many problems that restrict their sustainable development to meet the stringent environmental regulations [21]. The proposed liquid metal extraction−vacuum distillation method (LME−VD) consists of two simple steps: extraction and vacuum distillation [22]. The extraction step is simple dissolution in which the solid metals dissolve into the molten metal without generating any toxic waste and/or waste solutions. In the subsequent vacuum distillation step, the target extracted metal can be easily separated from the newly formed molten alloy, and the resulting volatiles is the added metals that can be reused in the former extraction process. Compared with the reported processes, the proposed method has the advantages of short flow and "zero waste" generation, which can be widely used to recycle other types of alloy scraps.

Figure 1 shows the Zn−Ni binary phase diagram. As shown in Fig. 1, Zn−Ni forms intermetallic alloys. Hence, it is expected that Zn has a strong chemical affinity to Ni and can readily dissolve Ni. The maximum solubilities of metals in molten Zn according to Zn−M (M=Ni, Co, Cr, Fe, Nb, Ti, Mo) at 700, 750, 800, 850, and 900 °C are summarized in Table 1. As illustrated in Table 1, there is a big difference in the solubility of metals in molten Zn, with nickel, cobalt and iron having large solubility than Cr and other refractory metals. Hence, the enriched nickel and refractory metals can be separated from superalloy scraps by recovering nickel with molten Zn as the extracting medium [23,24]. According to YAGI and OKABE [25], Ni diffused out of superalloy scraps into molten Zn, and they found that Ni and refractory metals contained in the superalloy scraps could be separated by utilizing the density differences between the Zn−Ni alloy and the refractory metals in molten Zn.

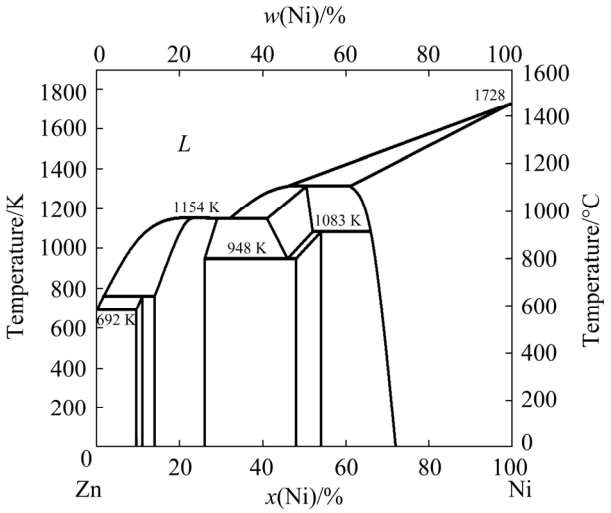

Fig. 1 Phase diagram of Zn−Ni binary system [26]

Table 1 Maximum solubility of metals in molten Zn (at.%)

Temperature/°C	Ni	Co	Cr	Fe	Nb	Ti	Mo
700	6.4	4.1	−	4.3	−	−	−
750	8.1	7.4	−	6.1	−	−	−
800	10.1	10.4	−	7.8	−	−	−
850	15.7	17.7	−	8.2	−	−	−
900	33.2	29.2	−	10.1	−	−	−
Reference	[26]	[27]	[28]	[29]	[30]	[31]	[32]

"−" means nearly insoluble.

Based on the reactions between Ni and Zn, Ni in the superalloy scrap can be selectively extracted by utilizing molten Zn to form Zn−Ni alloy, and then vacuum distillation is applied to removing Zn from Zn−Ni molten alloy. At present, there are few

studies on nickel extraction from superalloy scraps using molten zinc. To evaluate the optimum conditions for extracting Ni and separating the other alloy elements, the heating temperature, heating time and mass ratio of the zinc/superalloy are studied. Furthermore, molten Zn is employed as an extractant for discerning the extraction mechanism of Ni from superalloy scraps.

2 Experimental

2.1 Materials

The Inconel 718 superalloy was purchased from Dongbei Special Steel Group Co., Ltd., China. These superalloy bars (d=10 mm) were processed by electric spark machining into 2.0−3.0 g blocks. This work was conducted on Zn shots provided by Sinopharm Chemical Reagent Co., Ltd., China. Table 2 lists the chemical composition of the alloying elements in the superalloy and Zn samples used in this study, which were analyzed by inductively coupled plasma-optical emission spectrometer (ICP-OES: PS-6, Baird Corp, USA).

2.2 Procedure

The Ni-extraction experimental procedure is outlined in Fig. 2(a). The Zn shots and superalloy were mixed at a certain mass ratio in a quartz crucible (d=30 mm, h=50 mm). The extraction experiment was performed in a tube furnace (equipped with a vacuum air-removed system) with the purge of Ar gas (>99.999% pure). The heating rate was set as 10 °C/min from room temperature to the target temperature during the heating stage. After cooling, the obtained sample was cut through the Zn alloy region with a hacksaw. After reacting superalloy with the molten Zn, the upper part of the obtained sample (top 10 mm of the sample) was cut off, and these cut pieces were placed in a small quartz crucible (d=50 mm, h=60 mm), covered by a larger quartz crucible (d=80 mm, h=800 mm, with cover), followed by vacuum treatment at 900 °C for 360 min and pressure of 100 Pa. The composition of the sample obtained after the experiment was determined by ICP-OES (PS-6, Baird Corp, USA).

The schematic diagram of the LME-VD process is shown in Fig. 2(b). Extracting Ni from

Table 2 Chemical composition of Inconel 718 superalloy and Zn used in this study (wt.%)

Sample	Ni	Fe	Cr	Mo	Al	Co	Nb	Ti	Zn
Superalloy	52.6	17.9	19.7	3.6	0.4	0.4	4.8	0.6	0.0
Zn	0.0	0.0	0.0	0.0	0.1	0.0	0.0	0.0	99.9

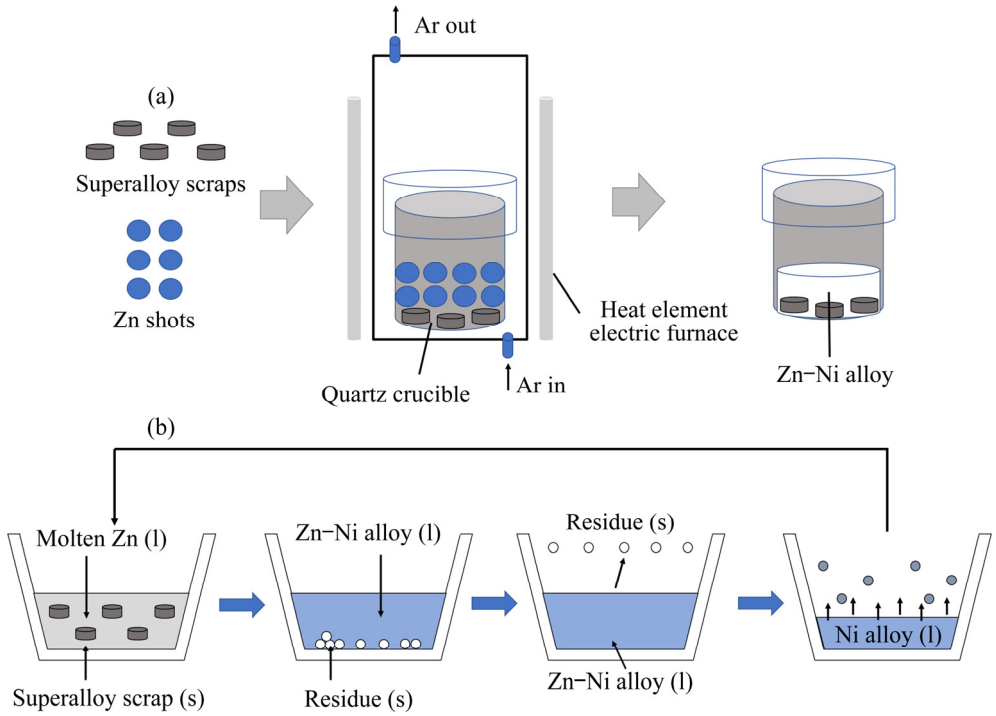

Fig. 2 Schematic illustration of Ni-extraction experiments (a) and schematic diagram showing Ni recycling from superalloy using molten Zn (b)

superalloy scraps is the focus of current research. It consists of the following three steps: (1) Ni in superalloy gets dissolved into molten Zn; (2) Separation of Zn−Ni alloy from the alloy residue; (3) Vacuum distillation-separation of Ni from the Zn−Ni alloy.

2.3 Analysis

The microstructure and composition of each phase in the obtained samples were analyzed by a scanning electron microscope, which is complemented by an energy dispersive X-ray spectrometer (SEM-EDS: TESCAN MIRA3, LMH-XMAX20). The top part of the obtained sample (top 15 mm of the sample) was cut off and its composition was analyzed using ICP-OES. The alloy was further analyzed by X-ray diffraction spectroscopy (XRD, D/Max−2500/PC, Rigaku, Japan) using the monochromatic target of Cu K for phase identifications. The volatilization of Zn in the experiment was ignored as it was negligible. The metal extraction rate could be calculated by Eq. (1). However, due to the unclear boundary between the original superalloy and the residual alloy, it was difficult to determine the mass of zinc in the residual alloy. In order to calculate the metal extraction rate, the mass of Zn in the alloy residue was ignored in the calculation process. Thus, the calculation of the metal extraction rate could be expressed as Eq. (2). However, the calculated value of the metal extraction rate was much higher than the actual value. The extraction of M was calculated as follows:

$$\eta_M=\{100w_M[(m_2-m_1-m_3)/w_{Zn}]\}/(m_1w_0)\times100\% \quad (1)$$

$$\eta_M\approx\{100w_M[(m_2-m_1)/w_{Zn}]\}/(m_1w_0)\times100\% \quad (2)$$

where η_M is the extraction rate of metals; m_1 is the mass of superalloy used in the experiment; m_2 is the mass of the sample after the experiment; m_3 is the mass of Zn in alloy residue; w_0 is the initial mass fraction of the metals in the superalloy; w_M is the mass fraction of the metal in the Zn alloy after cooling; w_{Zn} is the mass fraction of Zn in Zn alloy after cooling.

3 Results and discussion

3.1 Extraction

3.1.1 Effect of heating temperature

The effect of heating temperature was studied by fixing the heating time at 6 h, and the mass ratio of Zn/superalloy at 10:1, and the results are shown in Fig. 3. As seen, the extraction rate of Ni firstly increases with increasing temperature and reaches a plateau when the temperature is above 850 °C, during which the extraction rate of Ni exceeds 95%, suggesting that, most Ni in the superalloy can be dissolved into molten Zn at high temperatures. According to the data in Table 1, the maximum solubility of Ni in Zn increases with increasing temperature. Moreover, the diffusion and corrosion ability of Zn also increases with increasing temperature, which explains the results shown in Fig. 3. Figure 4 shows the backscattered electron image of the boundary between Zn and superalloy in the sample obtained at 700 °C. It can be determined from Fig. 4 that when the superalloy was immersed in molten Zn at 973 K (700 °C), only part of the superalloy was corroded. The SEM images of the sample show the clear boundary between the unreacted superalloy zone and the Zn alloy zone (Fig. 4(a)). The residual layer (Fig. 4(b)) contains Cr, Fe, Ni, Mo, Nb, and Zn, unreacted that Zn has corroded into the residual layer. The Zn alloy part mainly contains Zn, Ni, Fe and Cr (Fig. 4(c)), and the gray matrix is Zn. When heating the superalloy and Zn at a higher temperature of 800 °C, similar to 700 °C, the SEM images of the sample treated at 800 °C depict an obvious boundary. A wider residual layer can be observed in samples treated at higher temperatures (other conditions being the same), indicating a large reaction rate of the molten Zn to the superalloy. (Fig. 5(a)). EDS mapping of the left part indicates that the alloy section mainly contains Cr, Fe, Ni, and Nb, with hardly any Zn (Fig. 5(a)), but the Zn

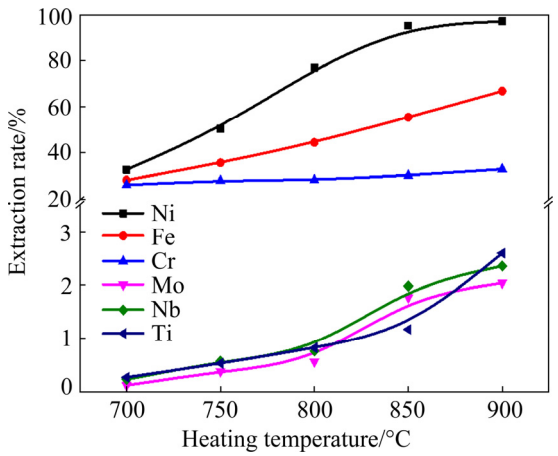

Fig. 3 Effect of heating temperature on extraction rate of various metals

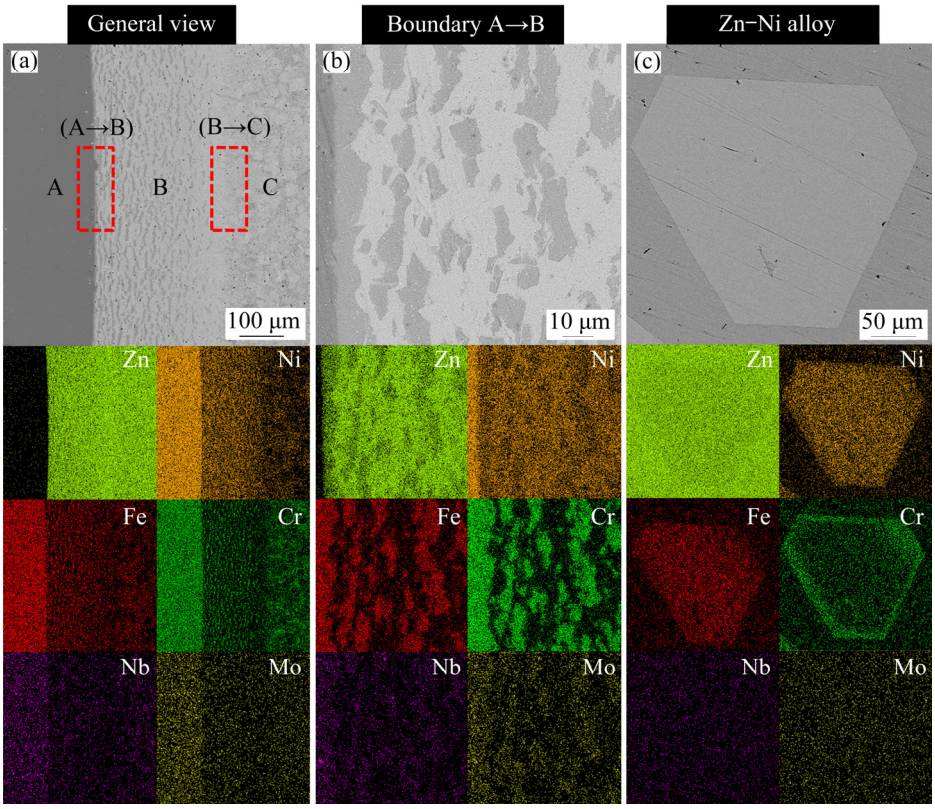

Fig. 4 Backscattered electron images of samples after heat treatment at 700 °C: (a) Boundary region between superalloy and Zn alloy; (b) Residual layer; (c) Zn alloy section

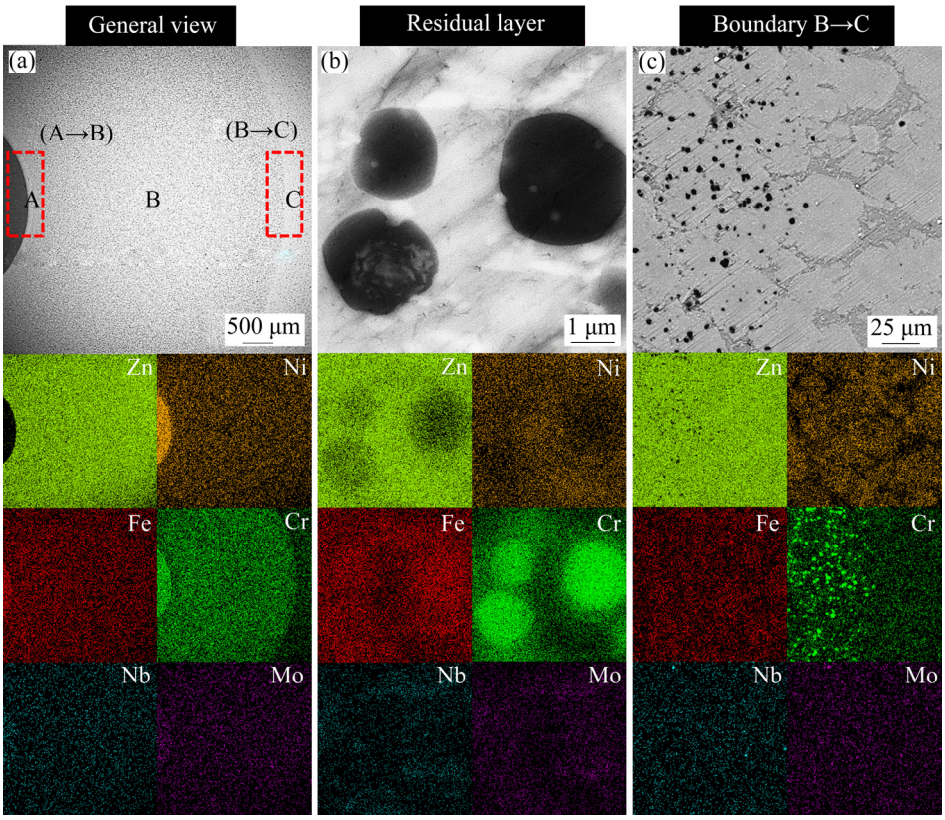

Fig. 5 Backscattered electron images of samples after heat treatment at 800 °C: (a) Low magnification showing presence of three zones; (b) Residual layer; (c) Boundary between residual layer and Zn−Ni alloy

alloy section mainly contains Zn, Ni and Fe (Fig. 5(c)).

As seen in Fig. 6(b), the calculated activity of molten Zn increases with increasing temperature in the range of 450−855 °C and then changes slightly with the continuous increase of temperature, which can explain the fact that the extraction rate of Ni increases with the increase of heating temperature. However, the boiling point of Zn (907 °C) is the limit of practical operating conditions. The evaporation rate of Zn above the boiling point is too fast, limiting the extraction rate of Ni and leading to a significant loss of Zn. While the extraction rate for Fe and Cr also increases with the increase of heating temperature, reaching about 56.8% for iron and 33.1% for chromium at 850 °C. The maximum solubility of Cr in Zn is low than 1 at.%, but the extraction rate of Cr is higher than 20% at all temperatures, which can be attributed to the dissolution of Cr in the Zn−Fe phase [28]. As for Mo, Nb, and Ti, their extraction rates also increase with temperature but are all less than 3% due to their low solubility in molten Zn at 850 °C [23,24]. Additionally, the volatilization of molten Zn is enhanced with increasing heating temperature. Hence, the heating temperature of 850 °C was used in the following experiments.

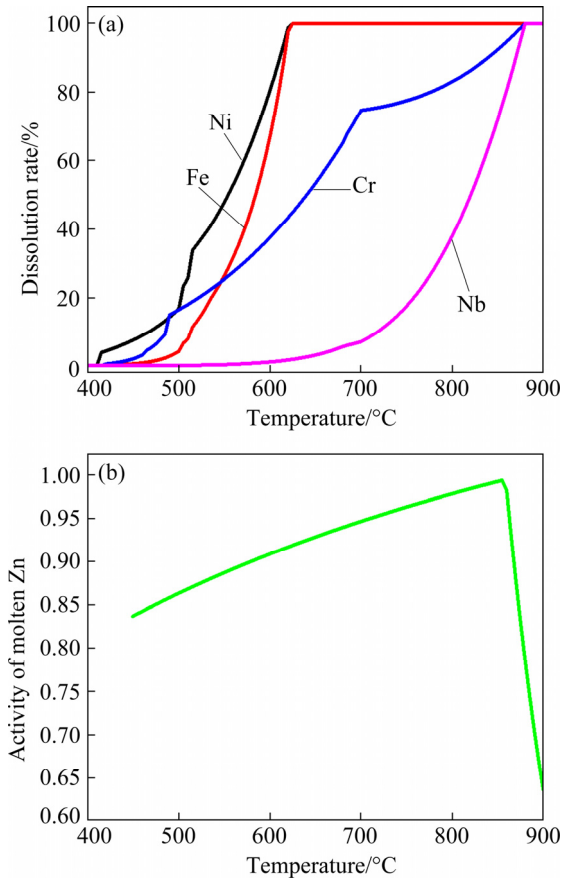

Fig. 6 Calculated results for simulating extraction process at different temperatures using Factsage software: (a) Calculated dissolution rate of metals in molten Zn; (b) Activity of molten Zn as function of temperature

In order to determine the influence of heating temperature on the dissolution of metals in molten Zn, the software Factsage was used to calculate the equilibrium components in the simulated extraction process, and the results are shown in Fig. 6. It can be seen from Fig. 6(a), that the calculated dissolution rate of Ni increases with increasing temperature, and reaches a plateau after around 620 °C. Further increase of temperature has a little effect on the dissolution rate of Ni, which is caused by the maximum solubility of Ni in molten Zn. As seen in Fig. 6(b), the calculated activity of molten Zn increases with the heating temperature from 450 °C to about 855 °C, and decreases sharply with a continuous temperature increase from 855 °C onwards. However, due to the limited heating time used in the experiments, the calculated dissolution rates of Ni and Fe are much different from the actual results, resulting from the calculated deviation and the inducted error of the selected database. The dissolution rates of Fe and Cr also increase with increasing temperature. The experimental data correspond well with the calculated results of Fe and Cr at different temperatures. However, the dissolution amounts of Nb and Mo are relatively low in the temperature range investigated.

3.1.2 Effect of mass ratio of Zn to superalloy

The effect of the mass ratio of Zn/superalloy was studied by fixing the heating time at 6 h and the heating temperature at 850 °C, and the results are shown in Fig. 7. The metal extraction rate is improved gradually with the increase of the mass ratio of Zn/superalloy. Therefore, a high Zn/superalloy mass ratio is beneficial for the extraction. Nearly 86.0% of the Ni in the superalloy could be extracted with a Zn/superalloy mass ratio of 6:1 at 850 °C, and up to 95.4% was extracted using a higher mass ratio of 10:1. Based on the composition of the superalloy, the amount of Zn used for the extraction of Ni from 1 g of superalloy is about 2.3 g, which means that the mass ratio of Zn/superalloy is 2.3:1, indicating that an excessive amount of Zn was added in the experiments with a

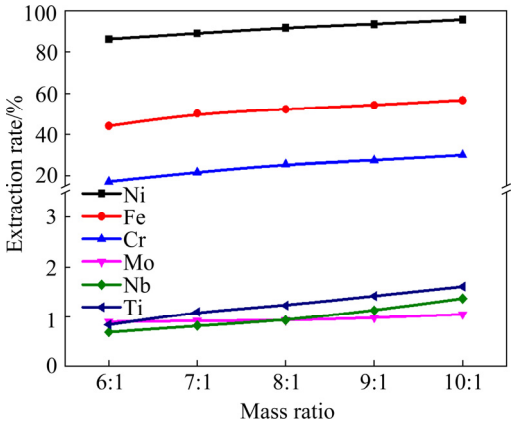

Fig. 7 Effect of mass ratio of Zn to superalloy on extraction rate of metals

Zn/superalloy mass ratio of 6:1 to 10:1. Hence, the extraction rate was improved slightly when the mass ratio of Zn/superalloy is in the range of 6:1 to 10:1. The calculation results of the dissolution of Ni in molten Zn correspond well with the experimental data. More Zn is present at a higher mass ratio during the extraction process, resulting in a larger concentration gradient between the residual layer with the molten Zn. This facilitates the diffusion of metals from the residual layer to molten Zn. As for Fe and Cr, the extraction rate also increases by increasing the ratio up to 10:1. Even at a ratio of 10:1, the extraction rates of Fe and Cr are 55.6% and 30.3%, respectively. Whereas the extraction of Nb, Mo, and Ti is still low with the change of Zn to alloy mass ratio. Considering the relative volume of molten Zn and the crucible size, a considerable amount of molten Zn was needed in this experiment to soak the superalloy completely. Therefore, a mass ratio of 10:1 was used in the following experiments.

In order to investigate the influence of the amount of Zn on the dissolution of metals from the original superalloy into molten Zn, we calculated the equilibrium composition with the addition of different amounts of Zn at 850 °C, and the results are shown in Fig. 8. As seen, the dissolution amount of Ni increases approximately linearly with the increase of the dosage of Zn (Fig. 8(a)) ranging from 1 to 150 g (mass ratio of 1:1.5), and continuous increase in the dosage of Zn results in negligible change, which is caused by the saturated solubility of Ni in molten Zn. The dissolution rate of Fe (Fig. 8(b)) is similar to that of Ni, which increases with the addition of more Zn. The calculated results of the dissolution of Ni, Fe, and Cr in molten Zn correspond well with the experimental data. It should be pointed out that the calculation results of Nb are quite different from the experimental data, since Nb metal is present in the original superalloy and the database selected in the calculation of Factsage has introduced errors.

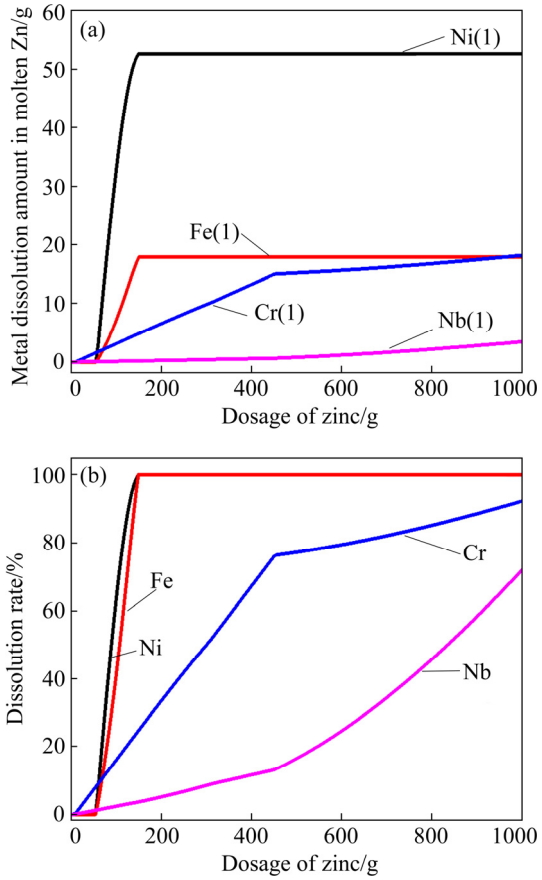

Fig. 8 Calculated results for simulating extraction process under different dosages of Zn at 850 °C by using Factsage software: (a) Dissolved amount of metal in molten Zn; (b) Calculated dissolution rate of metals in molten Zn

3.1.3 Effect of heating time

The effect of the heating time was studied using the heating temperature of 850 °C, and the mass ratio of Zn/superalloy of 10:1, and the results are shown in Fig. 9. The extraction rate of Ni increases with the increase of the heating time from 52.8% at 0.5 h to 95.4% at 4 h, but then shows a slight increase with the continuous increase of the heating time. As the reaction progressed, the concentration gradient of Ni between the reaction interface and the melt decreased, which resulted in a decrease in reaction rate. The extraction rates of Fe and Cr also increase with the increasing heating

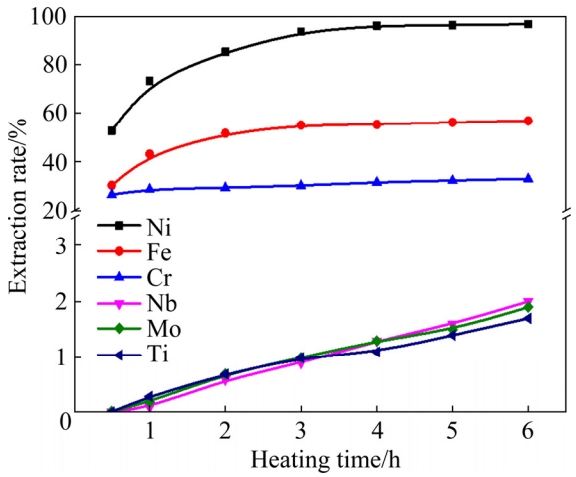

Fig. 9 Effect of heating time on extraction rate of metals

time, reaching about 53.1% and 31.6% after heating for 4 h, respectively. The extraction rate of Nb, Mo, and Ti is so low that they are hardly detected in the Zn alloy. Considering the fixed heating rate of 10 °C/min, it takes 85 min to reach the target temperature, and the gradual melting of Zn started when the temperature is above the melting point of 419 °C, indicating that the linear heating stage had 43.1 min for the melting of Zn. In addition, the dissolved elements (from superalloy) require adequate time for diffusion until reaching homogeneity, which ensures the accuracy of element extraction calculations. Therefore, there should be a relatively significant error for the experiments with a relatively short heating time.

Figure 10 shows the backscattered electron images of the interface between superalloy and molten Zn at 1123 K (850 °C) for various heating time between 30 and 240 min. As seen, the diffusion distance increases gradually with the proportionality of the heating time. The extraction process of Ni is a migration process of Ni from the original superalloy to the residual layer and then to molten Zn. The migration process is a diffusion process, including the transport of molten Zn to Ni in the residual layer, and the diffusion of Ni from the molten Zn with a high concentration to molten Zn with a lower concentration. At the initial extraction stage, the determinant stage is the dissolution of solid Ni into molten Zn. At the same time, with the extension of the heating time, the original superalloy will be eroded eventually, and the decisive factor is transferred to the diffusion of Ni from the molten Zn with high concentration into molten Zn with low concentration. The diffusion rate depends on the driving force generated by the decreasing concentration gradient of Ni with increasing heating time.

We can conclude that the optimum conditions for extraction of Ni are the heating temperature of 850 °C, the Zn/superalloy mass ratio of 10:1, and the heating time of 4 h. Under these conditions, however, a portion of the Fe and Cr are also extracted into the molten Zn.

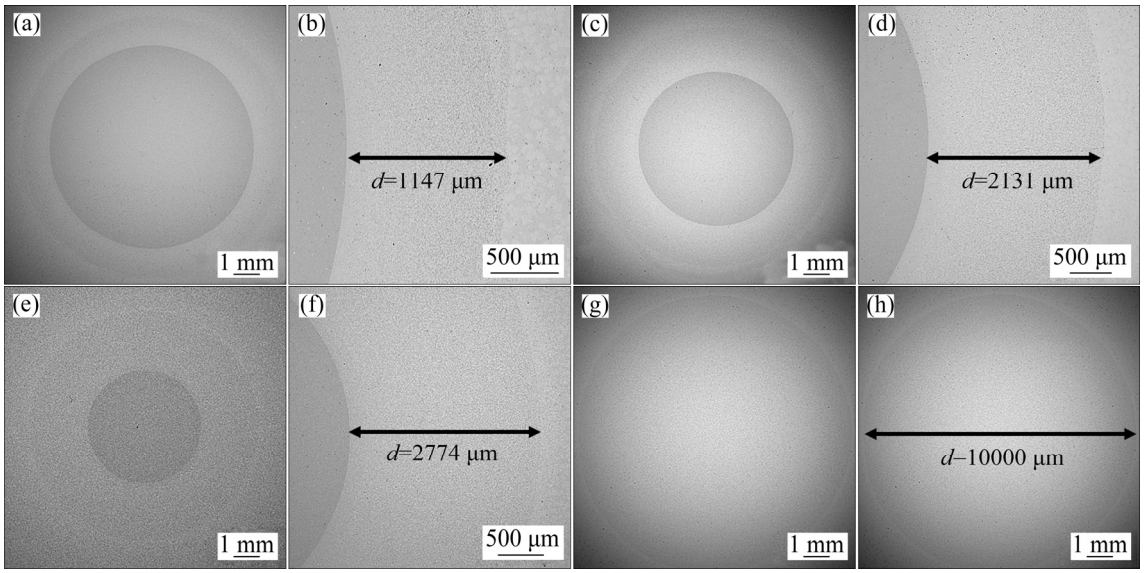

Fig. 10 Backscattered electron images of furnace cooling samples after heat treatment at 1123 K (850 °C) for different time: (a, b) 30 min; (c, d) 100 min; (e, f) 140 min; (g, f) 240 min (*d*: Diffusion layer thickness as plotted from SEM images)

3.2 Extraction mechanism

Figure 11 shows the backscattered electron image of the sample obtained after the heat treatment at 1123 K (850 °C) for 30 min. The SEM images show that several phases with different compositions are formed after the reaction of the superalloy with Zn at 1123 K (850 °C) for 30 min. As shown in Fig. 11(a), there is formation of an apparent boundary between the unreacted superalloy and solidified Zn. Table 3 lists the composition of Areas I, II, and III in Fig. 11(a). It can be determined that small amounts of Ni are extracted into molten Zn when the superalloy is soaked into molten Zn at 1123 K (850 °C) for 30 min. As seen, the light-colored zones are concentrated with Ni, Fe, and Zn (Fig. 11(c)), but the dark zones are concentrated with Cr and Zn, suggesting that the reaction between the molten Zn and solid superalloy results in the formation of Zn−Ni−Fe compounds within the Zn matrix. In the unreacted alloy scrap zone, the SEM images in different sample regions are similar in morphology. The EDS mapping of each part indicates that the alloy side mainly contains Cr, Fe, Ni, Nb, and hardly any Zn (Fig. 11(a)). In addition, the residual layer contains Cr, Fe, Ni, Nb, Mo, and Zn, and the granular shape phases are rich in Cr and Fe, namely (Cr, Fe) phase (Fig. 11(b)), Zn must pass through the residual layer to extract Ni from the original superalloy (Fig. 11(a)). The formed residual layer is the residue of superalloy after the loss of nickel metal. Based on the above analysis, the extraction of Ni is essentially the diffusion process of Ni from superalloy to molten Zn. During the heating process, the initial dissolution of Ni at the boundary between the original superalloy and the molten Zn occurs. The loss of Ni in the superalloys and the dissolution of other elements (especially the large amounts of Fe and Cr) in molten Zn facilitated the formation of the residual layers. Thus, the extraction of metals from superalloy can be divided into three main stages: the permeation of Zn into the superalloy, the diffusion of Ni in the residual layer, and the diffusion of metal in molten Zn [22].

Figure 12(a) shows the BSE image and EDS mapping results of the various regions from diffusion depleted zone to solidified Zn zone of the

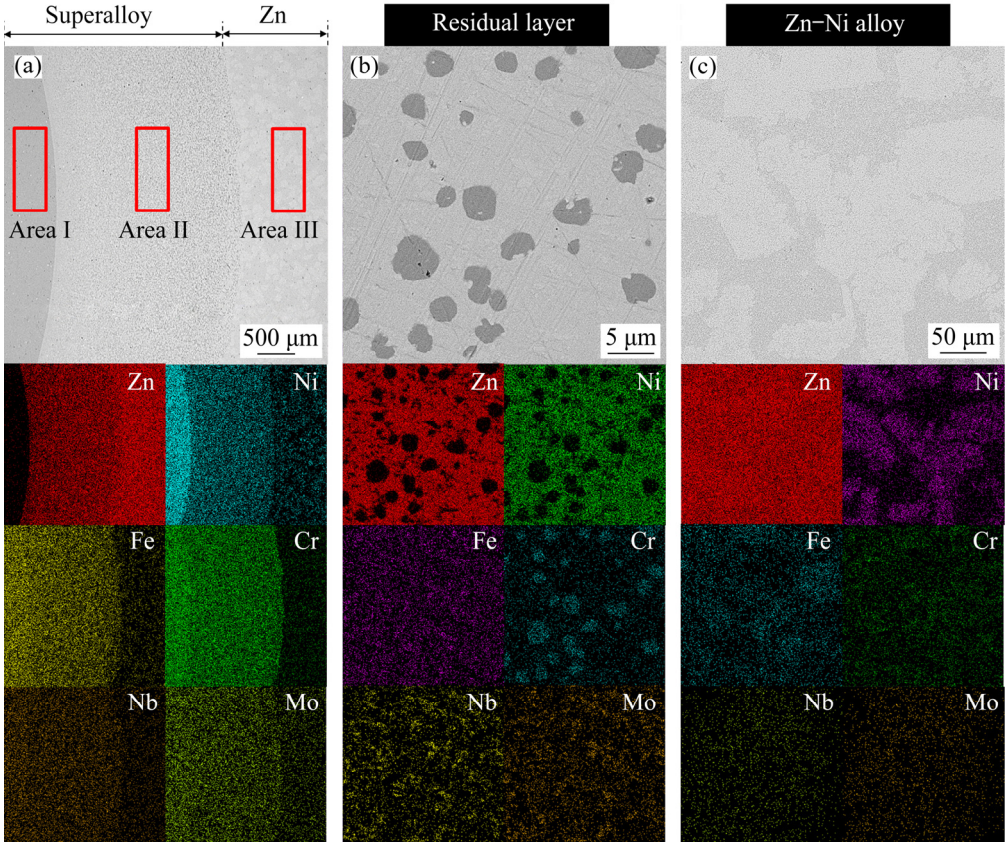

Fig. 11 SEM (BSE) images and EDS mappings of sample treated at 850 °C for 30 min: (a) Superalloy and Zn alloy with boundary; (b) Residual layer; (c) Zn−Ni alloy

Table 3 Analytical results of sample after Zn treatment at 850 °C for 30 min (wt.%)

Area in Fig. 11(a)	Ni	Fe	Cr	Mo	Al	Co	Nb	Ti	Zn
I	51.8	18.1	20.9	3.3	0.4	0.1	5.2	0.2	0.0
II	10.8	9.1	11.3	2.7	0.1	0.1	2.8	0.1	63.0
III	4.9	0.9	0.7	0.0	0.0	0.0	0.0	0.0	93.5

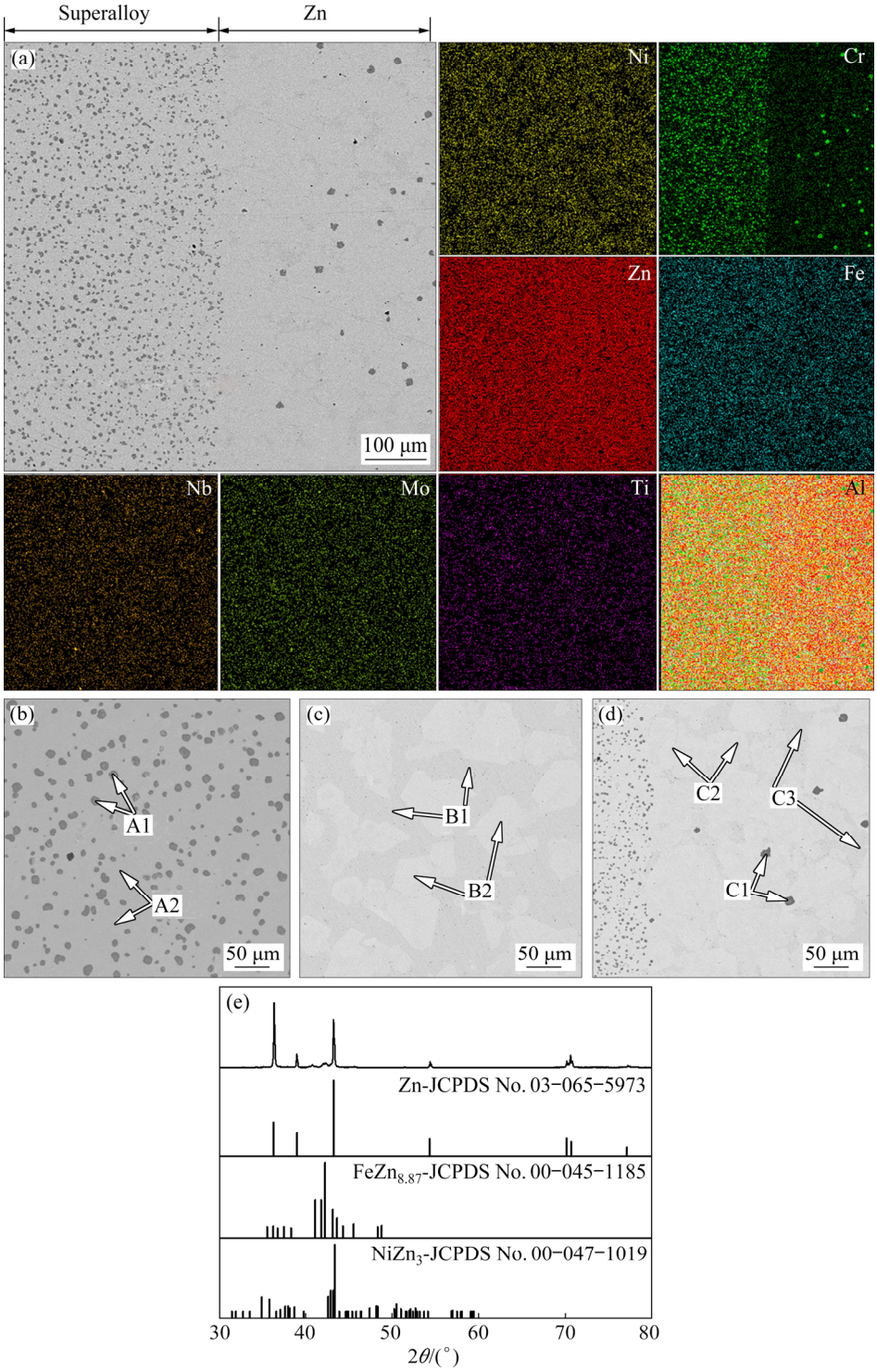

Fig. 12 Micrographs and atom distributions of various regions from residual layer to Zn−Ni alloy (a), SEM image of residual layer (b), SEM image of Zn−Ni alloy (c), SEM image of interface between residual layer zone and Zn−Ni alloy (d), and X-ray diffraction patterns of Zn−Ni alloy (e)

sample, reacted at 1123 K (850 °C) for 4 h. The EDS mapping of element distribution is carried out for Ni, Fe, Zn, Nb, Mo, Ti, and Cr. As shown in Fig. 12(a), when the Ni-based superalloy was dissolved in molten Zn, a large amount of Zn dissolved into the alloy. Entirely Fe, Cr, Mo, Ti, and Nb concentrated in the residual layer owing to their low solubility in molten Zn. Figures 12(b−d) show a section of the sample obtained after heating the superalloy and Zn ($m_{\text{superalloy}}$:m_{Zn}=1:10) at 1123 K (850 °C) for 4 h and cooling to room temperature. Table 4 shows the composition (mass fraction) of each phase determined by the EDS analysis. A concentrated Zn matrix (B1) and Zn−Ni−Fe phase (B2) exist outside the alloy (Fig. 12(c)). Intermetallic phases such as $CrFe_xMo_y$ (A1) and $ZnNi_xFe_y$ (A2) are observed in the alloy reaction layer (Fig. 12(b)). The chemical composition of the small particles in the C1 phase can be determined by EDS. As can be seen from the color and shape, the composition of the C1 phase is similar to that of A1.

Based on these experimental results, the refractory metals in the superalloy form a solid intermetallic compound ($CrFe_xMo_y$), and Ni and Fe in the superalloy will form a Zn−Ni−Fe metal compound with Zn, which is concentrated in the alloy residual layer. With the increase of time, a small amount of solid intermetallic compounds (C1) in the residual layer will diffuse into the extraction medium Zn (cf. Fig. 12 and Table 4: C1 phase). This compound can be separated from Ni because of its low solubility in molten Zn. Therefore, it can be seen from the experimental results that the nickel in the superalloy scraps can be extracted by molten Zn and separated from refractory metals. On the other hand, the results also show that a portion of Ni is not extracted into molten Zn because it is stabilized by forming an intermetallic alloy with Zn (cf. Fig. 12 and Table 4: A2 phase). The results shown in Table 4 and Fig. 12 indicate that the Ni concentrations in the Zn−Ni alloy in the molten Zn part (B1 and B2) are only 0.0 wt.% and 5.1 wt.%, respectively. Also, the concentrations of Ni in the Zn−Ni alloy in the alloy residual layer (A1 and A2) are 0.0 wt.% and 5.2 wt.%, respectively. When the Ni-based superalloy is dissolved in molten Zn, most Fe and Cr form intermetallic alloys with Zn and are enriched in the alloy residual layer due to their low solubility in molten Zn (cf. A1 phase in Fig. 12 and Table 4). Some Fe and Cr in the superalloy are dissolved into molten Zn and form intermetallic alloys (C1 in Fig. 12). The interface between the superalloy and solidified Zn is covered with a thin uniform layer of nickel (C2 in Fig. 12). In terms of microstructure, the high affinity of Zn to Ni enables Ni to quickly diffuse out of the superalloy into molten Zn and form the Zn−Ni−Fe phase in the cooling process. Figure 12(e) shows the XRD scans of solidified Zn obtained after the superalloy and molten Zn reaction at 850 °C for 4 h. As shown in Fig. 12(e), the solidification of zinc alloy consists of the matrix Zn phase, Zn−Fe alloy phase, and Ni−Zn alloy phase.

3.3 Zn separation from Zn−Ni alloy by vacuum distillation

After the superalloy has reacted in the molten Zn, the upper part of the sample (0 to 10 mm from the top of the sample) was cut off. Table 5 shows the ICP results for this piece. As shown in Table 5, the upper part of the obtained sample contained 92.8 wt.% Zn, 5.3 wt.% Ni, 1.2 wt.% Fe and 0.6 wt.% Cr. On the other hand, refractory metals such as Mo, Ti, and Nb were not detected.

Table 4 Analytical results of sample after Zn treatment at 850 °C for 4 h (wt.%)

Phase in Fig. 12	Ni	Fe	Cr	Mo	Al	Co	Nb	Ti	Zn
A1	0.0	15.9	75.7	2.7	1.2	0.0	0.0	0.0	4.5
A2	5.2	1.7	0.8	0.0	0.0	0.0	0.0	0.0	92.3
B1	0.0	0.0	0.0	0.0	0.0	0.0	0.0	0.0	100.0
B2	5.1	1.1	0.8	0.0	0.0	0.0	0.0	0.0	93.0
C1	0.0	22.9	47.1	13.1	1.1	0.0	11.7	0.4	3.7
C2	5.4	1.6	0.6	0.0	0.0	0.0	0.0	0.0	92.4
C3	0.0	0.0	0.0	0.0	0.0	0.0	0.0	0.0	100

Table 5 Analytical results of Zn-alloyed sample (wt.%)

Ni	Fe	Cr	Mo	Al	Co	Nb	Ti	Zn
5.3	1.2	0.6	0.03	0.0	0.0	0.07	0.0	92.8

Figure 13 shows the calculated vapor pressure of Zn and the other main components of the superalloy (Ni, Al, Co, Cr, Ti) as a function of temperature [33]. The vapor pressure of Zn at its boiling point (1180 K (907 °C)) is seven orders of magnitude higher than that of the other alloying elements in the superalloy. Therefore, Zn can be easily distilled and selectively removed by heating the obtained Zn−Ni alloy at around 1180 K (907 °C). In addition, the oxidation of Zn is prevented when it is distilled in inert gas. Therefore, Zn can be recycled and reused after Ni extraction. Thus, these properties of Zn make it possible to obtain concentrated nickel without producing any toxic wastes and/or waste solutions. Quartz crucibles containing residues were subsequently inserted into a Zn distillery, which was maintained under vacuum using a rotary pump. When the pressure inside the chamber dropped below 50 Pa, the temperature was raised to 1173 K (900 °C) at 10 °C/min and was maintained for 6 h. After heat treatment, the pressure inside the Zn distillation chamber was reduced to 15−20 Pa. The composition of each sample was analyzed by ICP-OES after cooling.

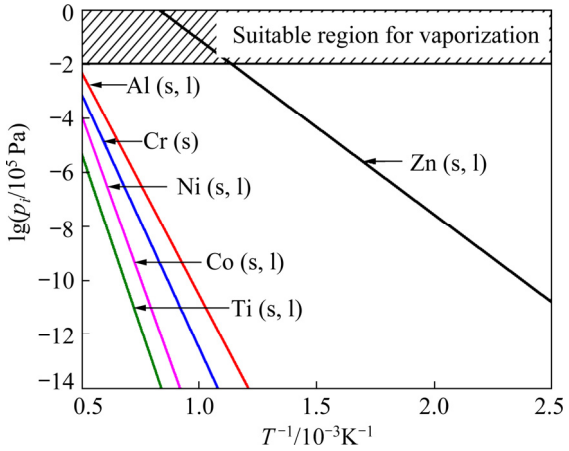

Fig. 13 Vapor pressures of selected metals as function of reciprocal temperature

Table 6 shows the composition of the metal deposits obtained in the low-temperature region and the metal residues collected in the high-temperature region. The deposits collected in the low-temperature region in the quartz reaction chamber were 99.9 wt.% Zn. Therefore, it is confirmed that Zn can be collected and reused as a selective collector for Ni recovery. The sponge-shaped metal obtained in the high-temperature region contained 1.1 wt.% Zn. Therefore, it was proved that the concentration of Zn in the upper part of the Zn-alloyed sample decreases from 92.8 wt.% to 1.1 wt.% by heating the sample at 1173 K (900 °C) for 6 h under vacuum.

Table 6 Analytical results of samples after Zn distillation experiment (wt.%)

Sample	Ni	Fe	Cr	Mo	Al	Co	Nb	Ti	Zn
Alloy	52.6	17.9	19.7	3.6	0.4	0.4	4.8	0.6	0.0
Residue	73.5	15.2	8.4	0.5	0.2	0.0	1.1	0.0	1.1
Deposit	0.0	0.0	0.0	0.0	0.0	0.0	0.0	0.0	99.9

Figure 14(a) shows the XRD patterns of samples obtained after Zn-distillation. All of the peaks can be identified as elemental $FeNi_3$ alloy and Cr_2Ni_3 alloy. After Zn-distillation, the extracted metals were collected at the bottom of the chamber, whereas the metal was deposited at the top of the quartz tube (Figs. 14(b, c)). It can be seen that the residues are in black flakes, and the metal deposited on the top of the quartz tube has a metallic luster.

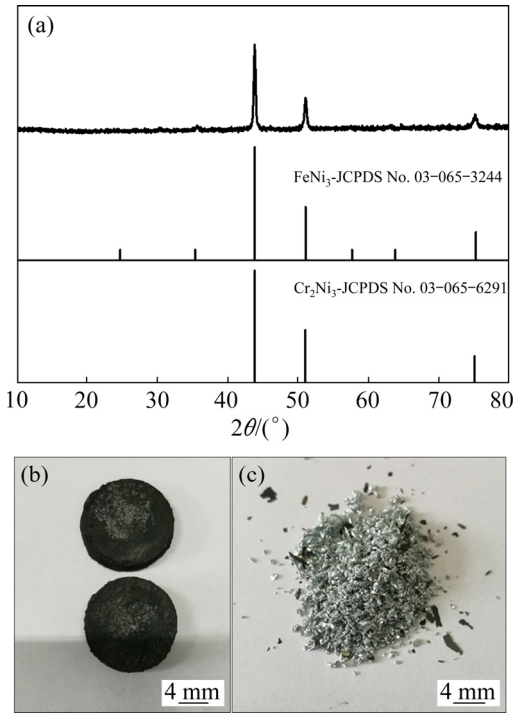

Fig. 14 XRD patterns and photographs of samples after Zn-distillation: (a) XRD patterns; (b) Residues collected in crucible; (c) Metal deposited in upper part of quartz tube

In the sponge-shaped metal residue distilled from Zn, the concentration of Ni is 73.5 wt.%, which is higher than that in the original superalloy. The sponge-shaped metal residue also contains Fe and Cr, and the total concentration of these two metals is 23.6 wt.%. As the chemical affinity between these elements and Zn is expected to be high [29], it may be unavoidable to retain a certain amount of Fe and Cr in sponge-shaped samples. Refractory metals such as Mo, Nb, and Ti hardly exist in the metal residue (1.6 wt.%), indicating that refractory metals can be separated from the Ni-based superalloy using the technique developed in this study.

The results show that it is feasible to extract concentrated nickel from superalloy scrap with molten Zn as an extraction medium. Moreover, these results indicate that the recyclability of zinc can be used to extract nickel.

4 Conclusions

(1) A new process with high efficiency and selective extraction of nickel from superalloy scraps using molten Zn as an extractant was proposed and studied.

(2) The experimental results indicate that the extraction rate of Ni increased with the increase of the heating temperature and heating time, while the mass ratio of Zn/superalloy had a slight influence on the extraction rate. More than 95 wt.% of Ni in the superalloy could be extracted into molten Zn under the optimum operating conditions.

(3) Vacuum heat treatment was carried out on the upper part of the Zn-alloyed at 1173 K (900 °C) to reduce Zn concentration in the sample from 92.8 wt.% to 1.1 wt.%. After the evaporation of Zn from the Zn-alloyed sample, the metal residue containing 73.5 wt.% Ni was obtained, in which the content of refractory metals could be neglected. These results confirm that molten Zn can effectively extract Ni in the superalloys.

Acknowledgments

The authors are grateful for the financial supports from the National Natural Science Foundation of China (Nos. 51922108, 51874371, 51904350), the Hunan Natural Science Foundation, China (No. 2019JJ20031), and the Hunan Key Research and Development Program, China (No. 2019SK2061).

References

[1] YANG Wan-peng, LI Jia-rong, LIU Shi-zhong, SHI Zhen-xue, ZHAO Jin-qian, WANG Xiao-guang. Orientation dependence of transverse tensile properties of nickel-based third generation single crystal superalloy DD9 from 760 to 1100 °C [J]. Transactions of Nonferrous Metals Society of China, 2019, 29: 558−568.

[2] ZHANG Peng, ZHU Qiang, CHEN Gang, QIN He-yong, WANG Chuan-jie. Grain size based low cycle fatigue life prediction model for nickel-based superalloy [J]. Transactions of Nonferrous Metals Society of China, 2018, 28: 2102−2106.

[3] ECKELMAN M J, CIACCI L, KAVLAK G, NUSS P, RECK B K, GRAEDEL T. Life cycle carbon benefits of aerospace alloy recycling [J]. Journal of Cleaner Production, 2014, 80: 38−45.

[4] WU Xian, WU Yong-qian, MENG Han-qi. Current status of superalloy scraps recovery and treatment technology [J]. China Molybdenum Industry, 2015, 39(01): 8−11. (in Chinese)

[5] DEBARBADILLO J J. Nickel-base superalloys; physical metallurgy of recycling [J]. Metallurgical Transactions A, 1983, 14(2): 329−341.

[6] SCHLATTER R. Melting and refining technology of high-temperature steels and superalloys: A review of recent process developments [J]. Superalloys A, 1972, 1: 1−40.

[7] CHEN Xi-chun, SHI Cheng-bin, GUO Han-jie, WANG Fei, REN Hao, FENG Di. Investigation of oxide inclusions and primary carbonitrides in Inconel 718 superalloy refined through electroslag re-melting process [J]. Metallurgical and Materials Transactions B, 2012, 43(6): 1596−1607.

[8] CHEN Zhang-jun, CHEN Zhen-bin, SUN Yuan, TANG Jun-jie, HOU Gui-chen, ZHANG Hong-yu, LIU Wen-qiang. Research progress and future development direction of recovery and reuse of superalloy scraps [J]. Materials Reports, 2019, 33(21): 3654−3661. (in Chinese)

[9] SRIVASTAVA R R, KIM M, LEE J, JHA M K, KIM B S. Resource recycling of superalloys and hydrometallurgical challenges [J]. Journal of Materials Science, 2014, 49(14): 4671−4686.

[10] KIM M S, LEE J C, KIM E Y, YOO Y S. Leaching of CMSX-4 superalloy in hydrochloric acid solutions [J]. Journal of Korean Inst. Resource Recycling, 2010, 19(5): 25−30.

[11] TAN Shi-xiong, SHEN Yong-feng. Recovery of nickel and cobalt from waste superalloy [J]. Engineering Chemistry and Metallurgy, 2000, 21(3): 294−297. (in Chinese)

[12] ZHAO Si-jia, CHU Guang, YANG Tian-zu. Review on recovery of nickel and other valuable metals from nickel waste [J]. Hydrometallurgy, 2008, 28(2): 72−76. (in Chinese)

[13] FAN Xing-xiang, XING Wei-dong, DONG Hai-gang, ZHAO Jia-chun, WU Yue-dong, LI Bao-jie, TONG Wei-fang, WU Xiao-feng. Factors research on the influence of leaching rate of nickel and cobalt from waste superalloys with sulfuric acid [J]. International Journal of Nonferrous Metallurgy,

2013, 2(2): 63−67.
[14] ZHOU Xue-jiao, CHEN Yong-li, YIN Jian-guo, XIA Wen-tang, YUAN Xiao-li, XIANG Xiao-yan. Leaching kinetics of cobalt from the scraps of spent aerospace magnetic materials [J]. Waste Management, 2018, 76: 663−670.
[15] LUEDERITZ E, SCHLEGEL U R, HALPIN P T, SCHNECK D L. Method for recovering rhenium and other metals from rhenium-bearing materials: US Patent, 20130078166 [P]. 2013-01-26.
[16] FERRON C G, SEELEY L E. Rhenium recovery: US Patent, 8956582 [P]. 2015-02-17.
[17] MENG Han-qi, WU Xian, CHEN Kun-kun, WANG Jing-kun. Recovery of rhenium from superalloy scrap by alkali melt-water immersion method [J]. Nonferrous Metals Engineering, 2014, 4: 44. (in Chinese)
[18] DASAN B, PALANISAMY B, LIPKIN D M. Recovery of rhenium for use as catalyst, involves oxidizing oxidation feedstock produced by increasing surface area of rhenium containing super alloy scrap into volatile rhenium oxide: US, 2011126673-A1 [P]. 2011-06-02.
[19] ATKINSON G B, NICKS L J. Leaching aluminum-superalloy melts with hydrochloric and sulfuric acids [J]. Conservation & Recycling, 1986, 9(2): 197−209.
[20] HILLIARD H E. Superalloy scrap embrittled by zinc vapour can be easily crushed for recovery of nickel cobalt and other metal valves: US, 4718939-A [P]. 1988-01-12.
[21] SINHA M K, MADARKAR R, GHOSH S, RAO P V. Application of eco-friendly nanofluids during grinding of Inconel 718 through small quantity lubrication [J]. Journal of Cleaner Production, 2017, 141: 1359−1375.
[22] CUI Fu-hui, WANG Gang, YU Da-wei, GAN Xiang-dong, TIAN Qing-hua, GUO Xue-yi. Towards “zero waste” extraction of nickel from scrap nickel-based superalloy using magnesium [J]. Journal of Cleaner Production, 2020, 262: 121275.
[23] VASSILEV G P. Thermodynamic evaluation of the Ni−Zn system [J]. Journal of Alloys and Compounds, 1992, 190: 107−112.
[24] GUO Xue-yi, ZHANG Chun-xi, TIAN Qing-hua, YU Da-wei. Liquid metals dealloying as a general approach for the selective extraction of metals and the fraction of nanoporous metals: A review [J]. Materials Today Communications, 2021, 26: 102007.
[25] YAGI R, OKABE T H. Recovery of nickel from nickel-based superalloy scraps by utilizing melting zinc [J]. Metallurgical and Materials Transactions, 2017, 48(1): 335−345.
[26] VASSILEV G P, ACEBO T G, TEDENAC J C. Thermodynamic optimization of the Ni−Zn system [J]. Journal of Phase Equilibria, 2000, 01(21): 287−301.
[27] VASSILEV G P, JIANG Ming. Thermodynamic optimization of the Co−Zn system [J]. Journal of Phase Equilibria and Diffusion, 2004, 25(3): 259−268.
[28] TANG Nai-yong, YU Xue-bing. Study of the zinc-rich corner of the Zn−Fe−Cr system at galvanizing temperatures [J]. Journal of Phase Equilibria and Diffusion, 2005, 26(1): 50−54.
[29] KIRCHNER G, HARVIG H, MOQUIST K R, HILLERT M. Distribution of zinc between ferrite and austenite and the thermodynamics of the binary system Fe−Zn [J]. Arch Fur Das Eisenhuttenwes, 1973, 44(3): 227−234.
[30] MOSER Z. The Nb−Zn (niobium−zinc) system [J]. Journal of Phase Equilibria, 1992, 13: 425−429.
[31] DOI K, ONO S, OHTANI H, HASEBE M. Thermodynamic study of the phase equilibria in the Sn−Ti−Zn ternary system [J]. Journal of Phase Equilibria Diffusion, 2006, 27: 63−74.
[32] ADACHI Y, ARAI M. Transformation of Fe−Al phase to Fe−Zn phase on pure iron during galvanizing [J]. Materials Science and Engineering A, 1998, 254(1−2): 305−310.
[33] BARIN I. Thermochemical data of pure substances [M]. 3rd ed. New York: VCH, 1995.

利用液态锌从镍基高温合金中一步选择性提取镍

田庆华[1,2,3]，甘向栋[1,2,3]，于大伟[1,2,3]，崔富晖[1,2,3]，郭学益[1,2,3]

1. 中南大学 冶金与环境学院，长沙 410083；
2. 有色金属资源循环利用国家地方联合工程研究中心，长沙 410083；
3. 有色金属资源循环利用湖南省重点实验室，长沙 410083

摘 要：采用熔融锌处理镍基高温合金并选择性地提取镍。研究加热温度、加热时间、锌与高温合金的质量比等因素对高温合金中金属提取率的影响。在加热温度为 850 °C，加热时间为 4 h，锌/高温合金的质量比为 10:1 的最优条件下，镍的提取率为 95.2%，铁的提取率为 55.4%，铬的提取率为 30.4%，而难熔金属(钛、钼、铌)的提取率较低。在后续的真空蒸馏过程中，蒸馏后得到的镍合金中含有 73.5%的镍(质量分数)。此外，蒸馏得到 99.9%的锌(质量分数)。研究结果表明，从镍基高温合金废料中直接提取镍是可行的。

关键词：高温合金；锌；镍；提取；真空蒸馏

(Edited by Xiang-qun LI)